Solvent Dependence of the Electronic Structure of I^- and I_3^-

Susanna K. Eriksson,[†] Ida Josefsson,[‡] Niklas Ottosson,[¶] Gunnar Öhrwall,[§] Olle Björneholm,[‖] Hans Siegbahn,[‖] Anders Hagfeldt,[†] Michael Odelius,[‡] and Håkan Rensmo[*,‖]

Department of Chemistry-Ångström, Uppsala University, Box 523, SE-751 20 Uppsala, Sweden, Department of Physics, Stockholm University, AlbaNova University Center, SE-106 91 Stockholm, Sweden, FOM institute AMOLF, Science Park 102, 1098 XG Amsterdam, The Netherlands, MAX IV Laboratory, Lund University, Box 118, 221 00 Lund, Sweden, and Department of Physics and Astronomy, Molecular and Condensed Matter Physics, Uppsala University, Box 530, SE-752 21 Uppsala, Sweden

E-mail: hakan.rensmo@physics.uu.se

[*]To whom correspondence should be addressed
[†]Department of Chemistry-Ångström, Uppsala University
[‡]Department of Physics, Stockholm University
[¶]FOM institute AMOLF
[§]MAX IV Laboratory, Lund University
[‖]Department of Physics and Astronomy, Molecular and Condensed Matter Physics, Uppsala University

Abstract

We present synchrotron-based I4d photoelectron spectroscopy experiments of solutions from LiI and LiI_3 in water, ethanol and acetonitrile. The experimentally determined solvent-induced binding energy shifts (SIBES) for the monoatomic I^- anion are compared to predictions from simple Born theory, PCM calculations, as well as multiconfigurational quantum chemical spectral calculations from geometries obtained through molecular dynamics of solvated clusters. We show that the SIBES for I^- explicitly depends on the details of the hydrogen bonding configurations of the solvent to the I^- and that static continuum models such as the Born model cannot capture the trends in the SIBES observed both in experiments and higher-level calculations. To extend the discussion to more complex polyatomic anions we also performed experiments on I_3^- and I^-/I_3^- mixtures in different solvents and the results are analyzed in the perspective of SIBES. The experimental SIBES values indicate that the solvation effects even for such similar anions as I^- and I_3^- can be rather different in nature.

TOC graphic.

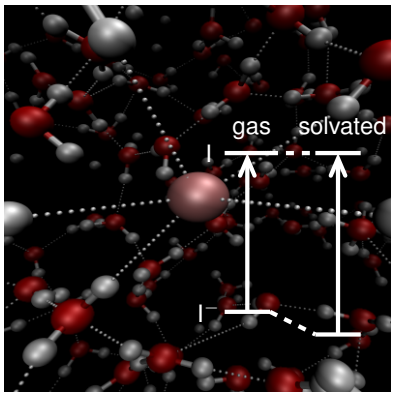

Keywords: Iodide, triiodide, solvation, core-level photoelectron spectroscopy, ab initio electronic structure calculations

1. Introduction

The use of iodine and its ions has many applications and was recently reviewed, as a celebration of the 200 years anniversary of its discovery.[1] Iodine and iodide can exist in many forms such as different ions, polymerized chains and of course molecular I_2.[2–4] Here we will focus on the simplest iodine ions namely iodide and triiodide which together form a well known redox couple, I^-/I_3^-. One specific example of the practical use of this redox couple is as the classic electrolyte for hole-transport in dye-sensitized solar cells.[5–7] In such systems a fundamental understanding of the solvation phenomena and energies involved are of great importance as a part of delineating the redox reaction mechanisms. Achieving this inevitably requires studies of the interaction between materials on the atomic length scales. Prime tools for such studies are methodologies based on X-ray techniques and advanced modeling.

There are plenty of studies in the literature dealing with solvation of iodide (and other halides) species both concerning electronic binding energies and segregation/migration at the surface and especially how the solvent molecules arrange around the ions as solvation shells[8–13] Previous EXAFS studies of iodide in solution show differences in solvation due to hydrogen bonding ability and coordination numbers[14] and another new EXAFS investigation discuss how I_3^- is distorted in aqueous solution.[15] Also photoelectron spectroscopy studies (PES) of I_3^- in ethanol have been reported and focus mainly on the fundamental spectroscopic details.[16] Moreover, PES studies of iodide in water clusters have been shown to be a suitable method for studies of solvation structures.[17] Previous theoretical studies of I_3^- in water and acetonitrile have also discussed the influence of hydrogen bonding and polarity of the solvent contra the symmetry of the I_3^- ion.[18,19]

The microscopic physical properties of the solvent such as the dipole moment and the ability to form hydrogen bonds, but also the resulting macroscopic dielectric constant will affect the solvation of the ions. It is therefore of interest to compare different solvents and investigate how these parameters affect e.g the solvation energies.[20] Obviously, one of the most studied solvents is water. Recently, we have used synchrotron based PES and advanced modeling to investigate the I_3^- ion in aqueous solution, where the solvent interactions tend to break the symmetry in the linear I_3^- ion

due to extreme I-I bond length fluctuations coupled to the solvent hydrogen bonding dynamics.[21] In aqueous solution, the geometric distortion of the I_3^- ion is a consequence of charge localization correlated with polarization in the solvent. To extend this study the present investigation includes other solvents besides water, namely ethanol and acetonitrile. In more polar solvents without hydrogen bonds (e.g. acetonitrile), the triiodide ion has been shown to be linear and symmetric.[22] Ethanol is a polar solvent with significantly lower density of hydrogen bonds than water. In that respect, it is an intermediate between water and acetonitrile.

In this paper, we specifically probe the I4d electronic energy levels in I^- and I_3^- and investigate solvent-induced effects using core-level PES in combination with electronic structure calculations and molecular dynamics (MD) simulations. The I4d core-levels in the I^- ions are probed in three solvents; water, ethanol, and acetonitrile while the core levels in I_3^- are studied in ethanol and acetonitrile and the solvent-induced binding energy shifts (SIBES) are analyzed.

2. Methods

2.1 Photoelectron spectroscopy

X-ray photoelectron spectroscopy (PES) measurements of LiI/LiI_3 solutions in water, ethanol, and acetonitrile were performed using synchrotron radiation at the undulator beamline I411 at the Swedish national laboratory MAX IV in Lund. The liquid samples were injected into the evacuated experimental chamber (~10^{-5} mbar) as a liquid micro-jet with a diameter of approximately 20 μm, by means of backing pressure from a HPLC pump. The Poynting vector of the X-ray radiation was perpendicular to the propagation of the liquid jet. The kinetic energy of the emitted photoelectrons was measured using a Scienta R4000WAL-analyzer mounted at 54.7° (the magic angle[23]) relative to the polarization plane of the linearly polarized radiation. The temperatures of the samples were estimated to be approximately 5 ± 5 °C. After passing the interaction region with the ionizing radiation, the liquid solutions were frozen in a cold trap cooled by liquid nitrogen. The experiment and the setup have been described in detail elsewhere.[24] The electrolyte solutions were prepared

fresh before each experiment, mixing chemicals with highly demineralized water, ethanol (99.5 %) or acetonitrile (99.8 %). All chemicals were purchased from Sigma-Aldrich (purity > 99%) and were used without further purification.

The I4d core-levels of the I^- and I_3^- ions were studied using a photon energy of 100 eV leading to a kinetic energy of the emitted electrons of around 50 eV. The spectrum of the I_3^- ion is partially overlapping with that of the 1s emission from the Li^+ ion. This overlap limits an accurate determination of the Li1s core-level binding energy as well as a detailed analysis of the shake-up feature[16] of I_3^-, which arises from simultaneously valence-excited core-ionized states. The binding energy calibration of the I4d region was performed by simultaneously measuring the photoemission from the corresponding evaporated solvent molecules and referencing the BE of the latter to literature data.[25] In recent publications dealing with liquid-XPS experiments in water the energy calibrations have been done using the HOMO peak of the liquid water instead of the gas line, as we have done here. However, one should notice that by dissolving ions the chemical potential for the solvent will be affected due to solvent rearrangements and therefore the solvent peak can be shifted with respect to the gas peak when concentrations (redox potentials) of the dissolved ions are changed.[8] The use of an internal reference in solutions of a single solvent partly remove effects from charge accumulation and thus gives internal energy calibration with high accuracy and reproducibility[26] but may lack information on specific surface charges. The use of the gas line is accompanied with an estimated uncertainty in the reported binding energies of I4d from I^- in the pure form and in the mixture with I_3^- of $\pm$0.1 eV. The uncertainty is most likely related to variations in surface charge of the jet due to frictional charging and varying photoionization density,[26] which influences the energy loss of electrons leaving the sample. In any case, the relative difference in binding energy between core-levels from I^- and I_3^- in mixed solutions have the accuracy of internal referencing and can hence be obtained with higher accuracy (i.e. <0.1 eV).

The binding energies are extracted from the experimental data by fitting to a Voigt profile. In the fitting, the core-hole lifetime broadening of the I4d state is assumed to be Lorentzian in nature, with a width of 0.175 eV taken from the literature.[27]

The I4d core-levels are atomic in character and we assume a constant spin-orbit splitting between the $I4d_{5/2}$ and $I4d_{3/2}$ lines, which is set to 1.70 eV both in I^-, I_3^- and the corresponding shake-up. The intensity ratios between the $I4d_{3/2}$ and $I4d_{5/2}$ are fixed to 0.75 taken from experimental data of pure LiI. This deviation of the branching ratio from the ideal statistical value of 2/3 has been observed also for the isoelectronic species xenon and can be explained by simultaneous electronic transitions to higher unoccupied states or to a continuum leading to lower intensity of the $I4d_{5/2}$ as compared to the $I4d_{3/2}$ line. The branching ratio depends on the photon energy used.[28]

In this study three different electrolytes were prepared by mixing LiI and molecular I_2 in different solvents and concentrations. In the first set of samples, equal concentrations of I^- and Li^+ in water, ethanol and acetonitrile are compared by preparing 0.5 M LiI solutions. Electrolytes with a 1:1 final ratio of I^- and I_3^- were also investigated with ethanol and acetonitrile as solvents by mixing 0.5 M LiI and 0.25 M I_2. Since the equilibrium between I^-, I_2 and I_3^- is strongly shifted towards I_3^- in organic solvents, it is assumed that all I_2 is consumed to form I_3^- when both I^- and I_2 are used in the preparation. Finally a solution containing mainly LiI_3 was made by mixing equal amounts of LiI and I_2 in ethanol giving a 0.50 M LiI_3 solution, with negligible I^- and I_2 concentrations. Experimentally it was not possible to obtain a stable jet for the acetonitrile and water solutions containing only LiI_3.

2.2 Computational details

In order to aid the interpretation of the experimental data and to shed light on the core-ionization process, we have calculated I4d binding energies for gas phase geometries and for configurations sampled in molecular dynamics (MD) simulations at different levels of approximation. The binding energies in the computed photoemission spectra were calculated as the vertical transition energies from the initial ground state to an electronically relaxed final ionized state, including relativistic effects, but neglecting the zero-point energy. Electronic structure calculations within multi-configurational self-consistent field (SCF) theory were performed with the MOLCAS version 7 program suite,[29,30] using wave functions constructed in the state-averaged complete active

space (SA-CAS)[31,32] framework and an all-electron basis set, adapted to relativistic calculations (ANO-RCC)[33–36] and contracted to VTZP quality. Through a second order perturbative treatment of these CASSCF wave functions, we also computed spectra including dynamic electron correlation (CASPT2)[37] for the gas-phase anions. The electronic structure was analyzed using the LoProp scheme[38] for charge analysis.

Relativistic effects are important in heavy elements like iodine and for the calculation of binding energies of core-levels. The relativistic effects were introduced in two steps, using the scheme implemented in MOLCAS. First, the set of multi-configurational states were calculated in a spin-free approach, using the scalar terms of the second order Douglas-Kroll transformation of the relativistic Hamiltonian.[39,40] Subsequently, the spin-orbit coupling matrix elements were computed, using the CASSCF (CASPT2) energies, as the interaction between the spin-free CASSCF (CASPT2) wave functions.[41,42] To obtain accurate spectra, it is necessary to design an active space that spans all states that couple strongly to each other.

In the electronic ground state and in the absence of solvent interactions, the I_3^- ion is linear with equidistant bond lengths.[22] The geometry was optimized (I–I = 2.91 Å) with the CASPT2 method including spin-orbit coupling, with the active space consisting of the 8 highest occupied valence orbitals and the LUMO, i.e. all 9 orbitals of nominal I5p character.

In the calculations of gas-phase I^- and I_3^- 4d spectra, we could evaluate the performance of a CASSCF wave function, involving only 4d orbitals in the active space, against calculations with an active space comprising the 4d orbitals and all occupied valence orbitals. (In both cases, the ground-state wave function of the anion, which is a closed shell singlet, was exactly equivalent to a Hartree-Fock calculation.) The (five/fifteen) highest roots of the final doublet states, corresponding to ionization from the 4d orbitals of I^-/I_3^- were computed in state-averaged calculations. For comparison to the experimental spectra, all transitions were given equal weight and a Gaussian broadening with a 1.0 eV full width at half maximum (FWHM) was applied to the computed binding energies.

Solute-solvent interactions were treated using two different models: An explicit cluster model,

with the ANO-RCC-VDZP basis set on the solvent, and an implicit polarizable continuum model (PCM).[43] In the latter, the response of the dielectric medium to the presence of the solute was calculated in equilibrium with the initial, singlet ground state. We neglect solvent relaxation in the final state, and the reaction field from the ground state calculations was added as a constant perturbation to the doublet states at the CASPT2 level in C_i symmetry. For I_3^-, the gas phase geometry was employed. The cavity sizes around the ion was obtained with the united atom topological model[44] using a radius around iodide of 2.05 Å. The default values of the dielectric constants in MOLCAS were used: ε = 78.39 (water), ε = 24.55 (ethanol) and ε = 36.64 (acetonitrile).

In order to sample solvation configurations with explicit solvent molecules, we performed classical MD simulations of LiI in acetonitrile, ethanol, and water solutions. For each solvent, 10 small clusters (containing the closest and most strongly interacting 6-9 water, 2-7 ethanol, and 11-15 acetonitrile molecules respectively) around I^- were extracted from MD simulations (evenly distributed over 100-200 ps long trajectories) and treated quantum mechanically. The solvent sphere radii for the selection of cluster sizes in the explicit solvent models were determined from the distance to the first minimum in the solute-solvent (I-O in water and ethanol and $I - CH_3$ in acetonitrile) radial distribution functions, which corresponds to the outer boundary of the first solvation shell. The results from the single-shell water cluster calculations were also compared with the binding energies obtained when adding a second solvation layer around I^- (32-41 water molecules).

We simulated the solvents using existing flexible force fields: the SPC water model,[45] OPLS-AA parameters for ethanol[46] and a six-site acetonitrile model,[47] and Li^+, Na^+ and I^- with the intermolecular parameters by Heinzinger.[48] Each simulation cell consisted of 100-300 solvent molecules, 1-2 anions and Li^+ or Na^+ as counterion for overall charge neutrality. The simulations used periodic boundary conditions in all directions and were carried out at constant volume and temperature. The time step of the MD algorithm was 2 fs, with a double time-step procedure (10*0.2 fs) for accurate integration of the fast vibrational motion based on fluctuations of intramolecular interactions.

In the presence of explicit solvent molecules, we were restricted to the CASSCF level of ap-

proximation for the quantum chemistry calculations and to an active space in which only the core orbitals were included. In order to guarantee that core-hole states were obtained, and avoid falling down into valence-hole states, the orbital rotations were constrained. This was done in a two-step procedure in which (1) the core-orbitals were optimized, freezing all other occupied orbitals to their respective shape from a previous Hartree-Fock calculation, and (2) the core-orbitals were kept fixed when optimizing the remaining electronic structure. Even though this freeze/thaw approach prevents direct mixing between the 4d orbitals and the valence, the two separate orbital spaces communicate through the virtual (unoccupied) orbitals. The procedure was evaluated at the CASSCF level for the isolated species in which we reproduce (within 5 meV) the results from calculations (without orbital constraints) that include both valence and core orbitals.

3. Results and discussion

In the following presentation of the core-level photoelectron spectra and the calculated binding energies, we will concentrate on effects from solute-solvent interactions and how the element specificity in X-ray based investigations can be used to understand electronic structures and associated geometrical effects. Initially the discussion focuses on solvation effects for the monoatomic I^- anion and in the end the investigation is broadened to contain the polyatomic I_3^- and some results on the mixed I^-/I_3^- electrolyte.

3.1. Solvation effects of I^- in different polar solvents

Spectra of the I4d core-levels, obtained by measuring 0.5 M solutions of LiI in water, ethanol, and acetonitrile, are presented in Figure 1. The observed doublet in the I4d spectrum is the result of a spin-orbit coupling in the partially filled core-levels in the core-ionized states. The energy splitting of the $I4d_{5/2}$ and $I4d_{3/2}$ levels in the experimental spectra is 1.7 eV, which can be compared to 1.64 eV for the calculated transitions.

Values of the core-level binding energies were extracted from the spectra in Figure 1 and col-

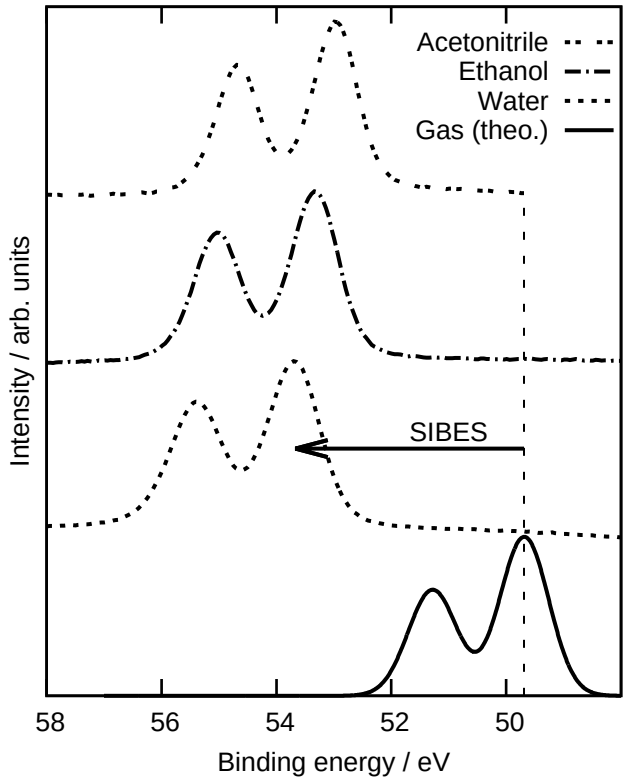

Figure 1: Top: Three different solutions with 0.5 M LiI in different solvents were measured. The spectra show the spin-orbit split I4d levels between 52 and 56 eV and contain information on the solvent-solute interactions. Bottom: The corresponding core-level binding energies of the isolated I^- ion, calculated with the CASPT2(+SO) method. The solvent-induced core-level binding energy shift (SIBES) indicated in the figure is calculated as the difference between the gas position and experimental solvated energies for I4d.

lected in Table 1. It is clear that the positions of the I4d peaks vary with the solvent. In comparison to the calculated gas phase binding energies, the binding energies of the I4d core-levels in solution are blue-shifted. The blue-shift is here analyzed as the SIBES. As far as we know, there are no published data on the 4d binding energies of gas-phase I^-. The I^- photoionization cross section has been measured in a merged beam experiment.[49] Unfortunately, the lack of sharp resonances in the I^- 4d excitation spectrum makes it difficult to exactly determine the ionization potential of the 4d levels, but the onset of increased photoionization cross section lies close to 50 eV, in good agreement with our calculated value. Assuming the same binding energy difference between I3d and I4d in the gas and solution phase a value of 49.3 eV can be estimated from experimental gas phase data and is close to our calculated value.[50,51]

In the interpretations it is important to note that the core-ionization processes discussed in the present work are very fast and the final state can be considered to be in the initial state nuclear geometry with a relaxed electronic structure in the presence of a core-hole. The dominant part of this electronic relaxation occurs inside the solute. However, effects from the surrounding solvent molecules will also contribute; in the comparison between the solution and gas phase binding energies, the solute electron relaxation will be similar and the difference can therefore be primarily ascribed to a change in the solvent polarization and solvent-induced polarization upon photoionization. Conceptually, the binding energies and specifically the SIBES can thus be considered to be the contribution of electronic interactions to the solvation energy without nuclear relaxation. Taking this reasoning one step further we note that the variations in the experimental values in Table 1 can be used to understand the solvation effects in electrochemical reactions where energy matching is of great importance . The SIBES values for I^- increase in the order acetonitrile (3.4 eV), ethanol (3.6 eV) and water (4.2 eV). In an attempt to shed some light on the origin of such variations in SIBES, both continuum solvation models and models based on specific intermolecular interaction are discussed below.

Table 1: The experimental data (in eV) for LiI water, ethanol, and acetonitrile solutions. The calculated theoretical value (CASPT2+SO) for I^- is used as a reference. The solvent-induced electron binding energy shifts (SIBES) are derived from the difference of experiments and calculations, derived from the Born model and calculated by sampling cluster calculations over configurations from MD simulations of LiI in water.

	Water	Ethanol	Acetonitrile	Gas (theory)
I^- ($I4d_{5/2}$)	53.8	53.2	53.0	49.59
I^- SIBES (Experimental)	4.2	3.6	3.4	
I^- SIBES (Born model with r=2.30 Å)	3.09	3.00	3.04	
I^- SIBES (Born model with r=2.05 Å)	3.47	3.37	3.42	
I^- SIBES (PCM)	5.33	5.18	5.25	
I^- SIBES (1 solvation shell)	2.80 ± 0.40	1.47 ± 0.37	1.36 ± 0.14	
I^- SIBES (2 solvation shells)	4.03 ± 0.47			

3.1.1. Continuum solvation models

To a first approximation solvation can be understood as the polarization of a dielectric (the solvent) by an ion (the solute) and described by the qualitative values obtained in the Born model. The Born model treats the solvated ion as a point charge Z_i and Z_f (initial and final states), placed inside a spherical cavity in a static continuum with the dielectric constant ε, and gives an estimate of SIBES when the ion is dissolved:

$$\mathrm{SIBES_{BORN}} = (Z_i^2 - Z_f^2)\frac{(\frac{1}{\varepsilon} - 1)e^2}{8\pi\varepsilon_0}, \tag{1}$$

where ε_0 is the vacuum permittivity and r the cavity radius.[52] The model contains only the ion-solvent interaction, neglecting the contribution from ion-ion and solvent-solvent interactions within the solvation shell. This simple model has previously been used to qualitatively rationalize trends observed in photoemission spectroscopy measurements.[53,54] Estimated SIBES derived from the Born model are presented in Table 1 where r is set to 2.30 and 2.05 Å.[55] As seen in Equation 1 an anion with -1 charge will have 0 contribution from the final state, hence we only have initial state effects contributing to the SIBES. For a cation, however, both the initial and final states will affect the SIBES and for a neutral species final state effects will dominate, as described in.[54]

The magnitude of the experimental SIBES for I^- is in general similar to that obtained from the Born solvation model (see Table 1) and are also similar to what has been reported previously.[53,56]

This supports the notion that SIBES can be considered to be the contribution of electronic interactions to the solvation energy without nuclear relaxation. However, when comparing the experimental SIBES in detail with those from the Born model, clear differences in the values are observed. The estimations derived from the Born model deviate by 0.4 to 1.1 eV from the experimental values and the relative order of the $SIBES_{BORN}$ and the experimental values is different. The Born model is approximate, hence it is not unexpected that the details in the SIBES from the experiments do not follow the variations in the dielectric constant as suggested by the Born model. For example, the SIBES is clearly smallest for I^- in acetonitrile, and we would therefore expect the dielectric constant (ε = 36.64) to be small compared to water and ethanol. This is true in the case of water (ε = 78.39) but not for ethanol (ε = 24.55). Thus, the simple Born solvation model (as used here for the initial and final states in the ionization process) which neglects effects of cavity shape, higher order electrostatic solute-solvent interactions and hydrogen bonding, and not captures the finer details in the solvation determining the binding energies for LiI in different solvents. For a more direct comparison to the results in the PCM model, described below, we also calculated the Born values for r set to 2.05 Å, which is the radius used for the iodide ion in the PCM calculations. The radius dependence in the Born model highlights the sensitivity and arbitrariness in the choice of cavity radii.

The fact that the Born-model cannot even qualitatively explain the experimentally observed SIBES serves as a motivation for the effort to perform ab initio calculations. In this way we hope to achieve a better understanding for the discrepancy by deriving the binding energies from the energies of the initial and final electronic states in the ionization process. Below, we present results from quantum chemical calculations on both implicit and explicit solvation models, and we begin with calculations performed using the polarizable continuum model (PCM).[43] In Table 1, we present simulated SIBES derived from quantum chemical based PCM calculations, in which the solution is represented by a single solute in a cavity in an infinite solvent, characterized by its macroscopic dielectric constant. The solute in the PCM model was modeled by quantum chemical CASPT2+SO calculations, which give accurate initial and final state energies of the solute, while

the solvent is only implicitly represented. The polarizable continuum model (PCM) can be viewed as an extension of the Born model, which takes the shapes of the cavity and the molecular charge distribution into consideration and lets the solute and solvent be mutually polarized.

We observe that the calculated SIBES in Table 1 of the I^- anion is slightly overestimated compared to the experimental data in Table 1. Considering the accuracy of the CASPT2+SO method for gas phase applications the discrepancy can be ascribed to the crudeness of the PCM continuum approximation. This crudeness is further manifested by a weak variation in the solvent dependence and specifically in the inadequacy to model relative changes in the SIBES when changing solvent.

3.1.2. Explicit intermolecular interaction - influence of hydrogen bonding

Since the continuum models discussed above lack the description of the local structure of the solvent, they are not able to give insights into the details in the solvent response. In particular, since the I^- ion is highly polarizable, it is important to consider explicit intermolecular interactions as well as charge-transfer contributions. For an anion, the solute-solvent interactions are more pronounced in the initial charged ground state than in the neutral core-ionized state, whereas for a neutral molecules the charged final state has stronger solute-solvent interactions than the initial neutral ground state. Therefore, we also performed theoretical modeling by sampling solvation structures from molecular dynamics (MD) simulations and by using a cluster approach.

In order to capture the short-range solvation interactions, the ion-solvent cluster should at least comprise the first solvation shell around the solute. We based the cluster sizes on ion-solvent radial distribution functions (RDFs), calculated from the MD trajectories (each in total 1-2 ns, after equilibration). Since the RDF gives the probability of finding two different atom types separated by the distance r, relative to a uniform distribution, the RDF maxima in Figure 2 are directly related to the solvation shells of I^- in the different solutions.

The I^-–solvent RDFs in water and ethanol display a well-defined maximum in the I^-–H RDF, a clear signature of hydrogen bonds coordinating the I^- ion. Due to the large dipole moment of the acetonitrile molecule, its positive end is also likely to point towards the I^- ion, but since the

acetonitrile dipoles tend to align in an antiparallel fashion, the structure is more disordered.

The first minima in the RDFs in Figure 2 were used to define the first solvation spheres, thus creating fixed-radius clusters. The resulting water clusters included all solvent molecules for which the oxygen and the solute were located no more than 4.2 Å apart. In ethanol, the I-O distance (5.0 Å) set the cluster size. The I^--acetonitrile clusters contained all solvent molecules with either carbon atom situated within 6.25 Å from the I^- ion. For I^- in aqueous solution, the cluster size was also extended up to the second ion-oxygen minimum (I–O: 6.6 Å), i.e. forming on average two hydration shells.

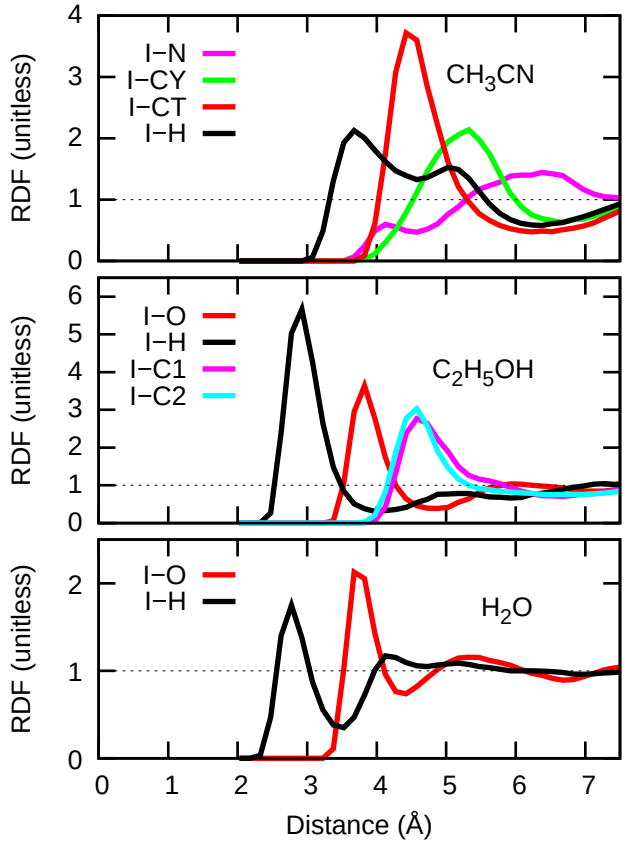

Figure 2: Radial distribution functions of water (bottom), ethanol (middle), and acetonitrile (top) about I^- from classical MD simulations of the solutions. The RDF minima are used to define solvation spheres and cluster sizes for the spectral sampling. CY denotes the RDF between I^- and the cyanide carbon atoms, and CT the RDF between I^- and the methyl carbon atoms in acetonitrile. C1 is the carbon bonded to the hydroxyl group and C2 the carbon of the methyl group in ethanol.

Based on the results from this quantum chemical level description (CASSCF+SO, i.e. neglecting dynamical correlation) in Table 1, we will in the following refer to the observed directed

electrostatic interaction between the negative I^- ions and the OH-group as hydrogen(H)-bonding, since this weak chemical bond have similar structure and origin as the H-bonding between the solvent molecules.

Attractive solvent interactions, in particular hydrogen bonding in water and ethanol solutions, are important for the structure in the solvation cage. In the cluster calculations, solvent molecules around the ion in the first and second solvation shells were included. The experimental I4d peak widths increase from 0.9 eV to 1.0 and 1.1 eV in the series acetonitrile, ethanol, and water. Theoretically the sampled structures give larger variations in binding energy for water and ethanol compared to acetonitrile. The higher sensitivity of the binding energy to the geometry of the water and ethanol clusters is ascribed to the hydrogen-bonding interactions in these solvents, which result in short-range solute-solvent interactions.[54]

The short-range interactions are easily observed in the SIBES from the quantum chemical cluster calculations. Although the discrepancy in the magnitude in the SIBES indicates some general weakness of using a limited cluster size we note that only when including specific I^- solvent interactions in the theoretical modeling we observe substantial variation in the SIBES values for different solvents as well as a trend showing the largest SIBES for the water solution and the smallest SIBES for acetonitrile. This result clearly illustrates the importance of differences in explicit hydrogen bond formation in order to understand SIBES for the I^- ions in different solvents. In water the ions are dissolved in an extended three-dimensional network of hydrogen bonds. The close interactions and strong hydrogen bonding between the ions and the water molecules lead to large solvation energies. Ethanol exhibits tendencies to form chains and clusters of hydrogen bonds in the solution whereas in acetonitrile the solvent structure is determined by dipolar interactions. These interactions are reflected in the radial distribution functions from the MD simulations in Figure 2, which reveal a less ordered acetonitrile structure around I^- in comparison to the distinct solvation shells of water and ethanol. Again, this implies that the differences in SIBES can be ascribed to the characteristics of the attractive intermolecular interactions for the respective solvents.

It could be noted that the limited cluster size yields too small solvent-induced binding energy shifts, since the model does not capture all the long-range effects: solvent polarization and distribution of the solvent dipoles by the solute, which are adapted to and stabilize the electronic ground state. In the case of water an estimate of the limitations in the cluster calculations was made by including a second solvent shell around I^-. In this case the SIBES increased from 2.8 eV to 4.0 eV for I^- as seen in Table 1. A single solvation layer is clearly insufficient to account for the experimental SIBES, but we observe a clear improvement in comparison to experiment and a reduction in the fluctuations when adding the second solvation shell. The importance of including both the closest solvent molecules and the long-range solvent response to ionic solutes has been described previously.[57] Unfortunately, for increased cluster size the multi-configurational SCF calculations became too demanding and we were unable to evaluate the convergence of the theoretical SIBES with respect to cluster size. We aim in future investigations to evaluate an alternative computational framework, employing QM/MM or density functional theory (DFT), which are applicable to larger models. Finally, we calculated the SIBES for a single I^-–water cluster (including the first layer of water molecules) surrounded by a polarizable continuum (PCM), which increased the SIBES for the specific geometry from 2.8 eV (QM cluster) to 5.61 eV (QM+PCM), i.e. almost 0.3 eV higher than the SIBES obtained with PCM without explicit solvent molecules.

3.2 Solvent effects for I_3^- in solution

To obtain further information on how solvent-ion interactions develop from a monoatomic to a polyatomic ion, the I_3^- ion in the different solvents were investigated. As discussed in a previous paper, the effects from hydrogen bonding in water solution were specifically important and induced large asymmetries in the I_3^- ion.[21] In the following we turn to compare the solvation in acetonitrile, a strongly polar but non-hydrogen bonding solvent, and ethanol, in which hydrogen bonds are present. Before analyzing the experimental spectra of I_3^- in solution, the results from the quantum chemical calculations of the isolated I_3^- ion are presented as a basis for the following discussions.

3.2.1. Calculations on the isolated I_3^-

The geometry optimization of the isolated I_3^- ion (yielding a linear and symmetric structure) and the I4d PES spectrum simulation of the the I_3^- ion were performed within the CASPT2+SO framework. The population analysis shows that the central atom in the I_3^- ion is close to net neutral, the negative charge being equally distributed between the atoms at both ends (the terminal atoms). Valence charge transfer from the central to the terminal iodine results in more tightly bound 4d electrons on the central site. From calculations with no symmetry restrictions we see that the core-holes are localized on individual I atoms in the different core-ionized states, and that spin-orbit coupling essentially does not mix electronic configurations with the core hole on different nuclei. Each state can therefore be said to have a definite terminal and center character, depending on the orbital from which ionization occurred. The calculated (CASPT2+SO) difference in binding energy between the terminal and central atoms in I_3^-(g) is 2.0 eV.

The theoretical energies of the final core-ionized states (including spin-orbit coupling), relative to the initial state of the I_3^- are shown as discrete lines in the spectrum in panel b in Figure 3. In panel a in Figure 3, we give the detailed assignment of each line and compare the core-ionized state before and after spin-orbit coupling is introduced, which is essential to describe the experimental spectrum. We also notice that the interaction between electrons in the 4d orbitals on the central iodine and the adjacent nuclei depends on the m_l quantum number of the orbital: it is the largest for orbitals spatially oriented along the molecular axis ($m_l = 0$) and the smallest for orbitals perpendicular to it ($m_l = \pm 2$). This gives an additional contribution to the width of the central peak (at most 0.5 eV) in the spectrum in panel b in Figure 3, but does not contribute to the broadening of the peaks from the terminal atoms.

However, generally the gas-phase lines in experimental spectrum can often be broadened by vibrational effects and the core-hole life-time. In terms of lifetime the Lorentzian contribution is about 0.175 eV.[27] In terms of vibrational effects the largest vibrational broadening is expected for the terminal component of the spectrum, which we also observe in the experimental data. In an attempt to estimate the contributions from intramolecular vibrational broadening to the line

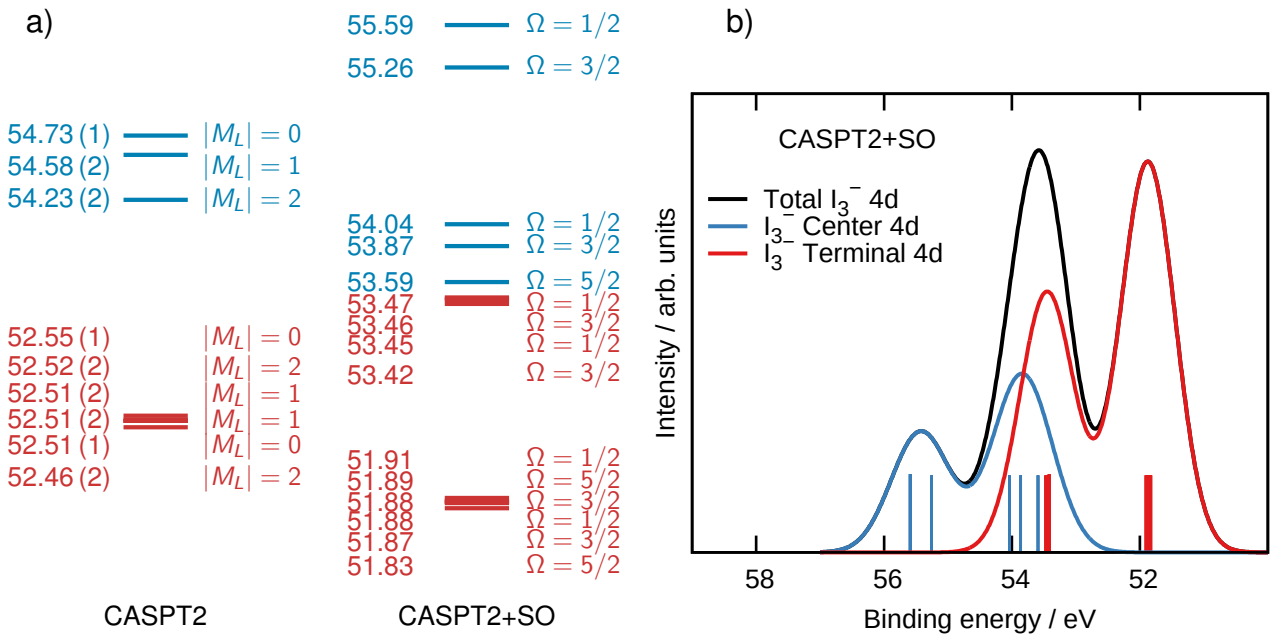

Figure 3: Calculated energies of the core-ionized states of I_3^-, relative to the initial state energy (in eV). The 15 possible states, corresponding to a core hole in each of the I4d orbitals respectively, are shown in panel a. Due to the excess charge on the terminal sites, electrons have lower binding energy (red states) than core electrons localized in orbitals at the central iodine (blue states). The spin-orbit coupled states (CASPT2+SO) which form the photoemission spectrum in panel b are calculated from the interaction between the spin-free states (CASPT2).

width, we performed scans along the harmonic vibrational normal modes in the I_3^- molecule (at the CASSCF+SO level, i.e. without inclusion of dynamical electron correlation). The resulting potential energy surfaces are shown in Figure 4. We can obtain a line width by projecting the ground state distribution, which for each mode is modeled as the square of the lowest vibrational wave function, onto each core-ionized state and monitoring the resulting binding energy distribution. The analysis shows that the major source of vibrational broadening of the terminal peaks (FWHM = 0.6 eV) is the asymmetric stretching of the molecule, while this mode does not cause any significant broadening of states with the core hole located on the central site. As Figure 4 indicates, this is due to that the shape of the energy surfaces of the terminal core-ionized states is considerably different from the harmonic ground state potential along the asymmetric stretching coordinate, whereas the curvature of the energy surfaces of the central core-ionized states is similar to that of the ground state. In the same sense, we observe that the central core-hole line width broadening

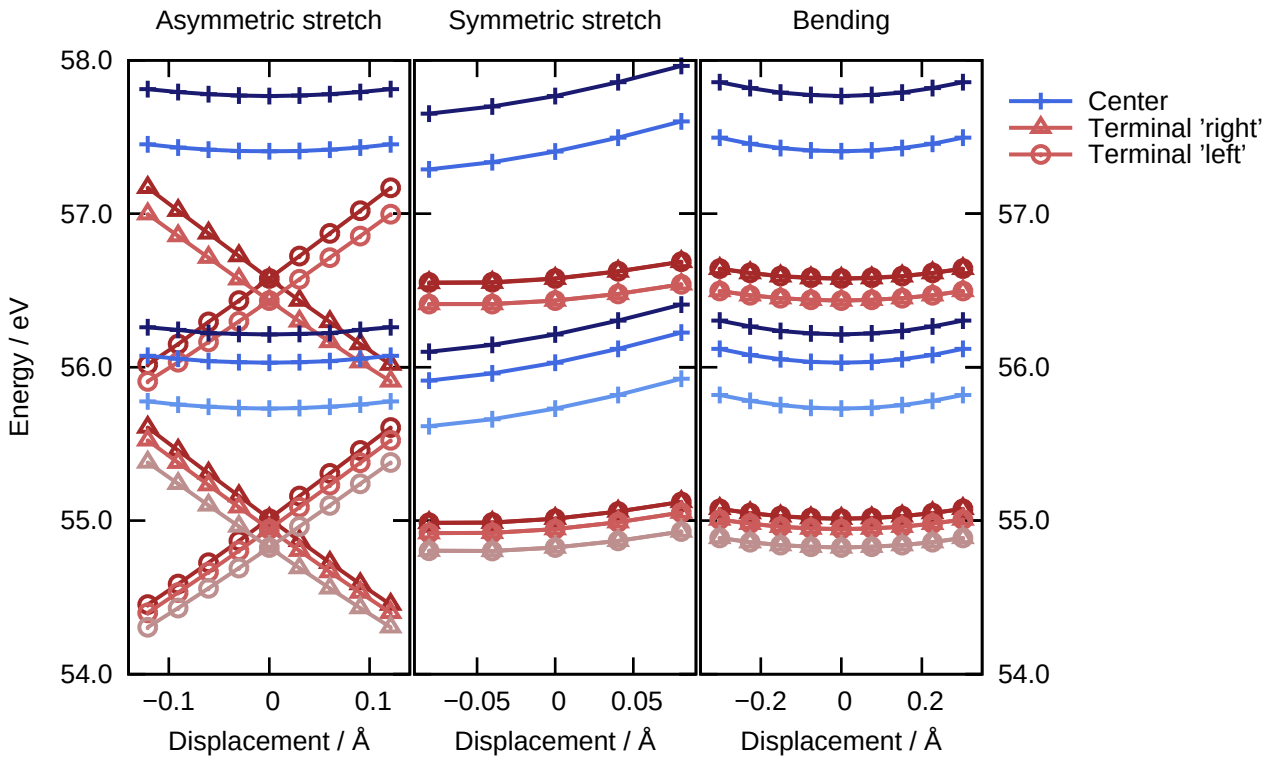

Figure 4: Potential energy surfaces of the 4d core-hole states of the neutral I_3 molecule relative to the ground state potential minimum of I_3^-, calculated (CASSCF+SO) along the vibrational coordinates of the system. (The bending mode is doubly degenerate.) Red curves correspond to core-ionized states with the hole localized on the terminal iodine and blue to states with a center site core hole. The contribution to the line width from each mode depends on the shape of the final state surface with respect to the initial state and the width of the ground state wave packet.

due to symmetric stretching (0.07 eV) is larger than the corresponding broadening of the terminal peaks (0.03 eV). The calculation shows that the two degenerate bending modes essentially do not contribute to the vibrational broadening of any of the lines in the I_3^- spectrum.

3.2.2 Experimental spectra of the I_3^- ion

By mixing equal amounts of LiI and I_2 in ethanol it was possible to measure experimental spectra on a liquid jet containing the anion I_3^- only and thus without I^-. The experimental spectrum of the I4d levels in panel b in Figure 5 contains a main structure between 52-58 eV, originating from the 4d levels in I_3^-. At binding energies over 58 eV in Figure 5 the Li1s peak is found just as in the case of pure LiI. Between the peaks from ionization of the I4d and Li1s core-levels additional features

appear compared to a spectrum containing only LiI. These features (one of which is at roughly the same position as Li1s) are due to simultaneous core ionization and valence excitation, known as a shake-up process. Previous studies[16] on I3d photoemission spectra of I_3^- propose that the satellite is likely to originate from a shake-up excitation of the highest occupied orbital (HOMO), which is a σ_g orbital, to the lowest unoccupied (LUMO), of σ_u type. Since all orbitals on the central atom are symmetric with respect to the inversion center of the molecule (g symmetry), this ($g \rightarrow u$) excitation is symmetry forbidden in ionization from the central iodine. Therefore, only core ionization from the terminal sites, where symmetry is broken due to the core hole localization, can be accompanied by a shake-up. Note that the shake-up features observed in the experimental spectrum are not modeled in the theoretical spectrum in this study.

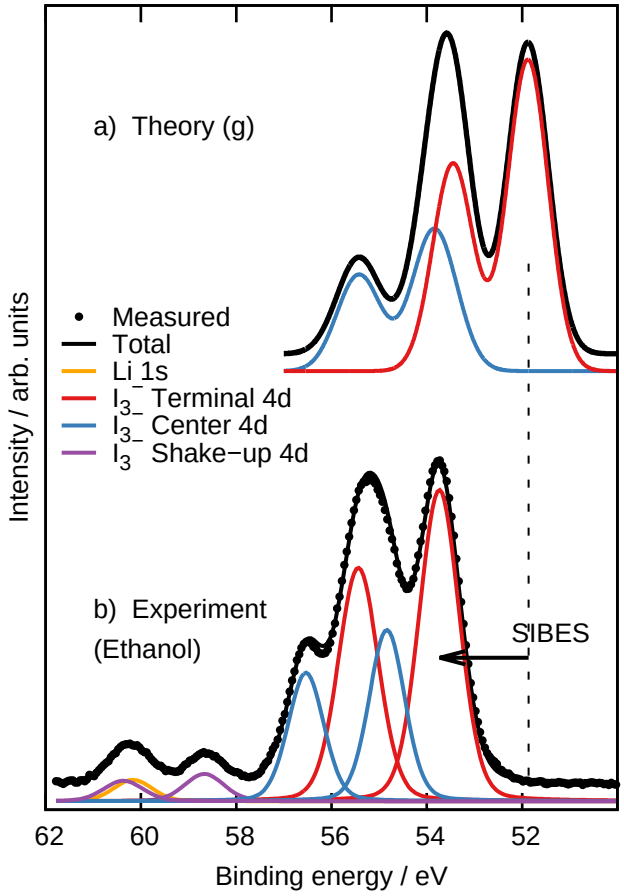

Figure 5: The I4d photoemission spectra of only I_3^- as measured in LiI_3 in ethanol and the CASPT2+SO calculated spectrum of I_3^-(g). The experimental spectrum is adapted from our previous paper.[21] The decomposition into different contributions is discussed in the text.

Motivated by the theoretical calculations above and as described in the experimental section, the main structure was decomposed into contributions from the center and the terminal iodine in the fitting and the resulting excellent fit quality upon such a spectrum deconvolution suggests that the I_3^- ion in ethanol is indeed symmetric. As in the case of I^- (discussed above) the SIBES for I_3^- can be estimated by comparing the peak position of the dissolved ions with the theoretical calculated position of the gas form of the ion.

Table 2: Experimental data of the binding energies and derived solvent-induced binding energy shifts (in eV) extracted from the spectrum of the ethanol solution containing LiI_3, presented in Figure 5. The theoretical binding energies are calculated at the CASPT2+SO level.

	Ethanol	Gas (theory)
Binding energy I_3^- (terminal $I4d_{5/2}$)	53.7	51.87
Binding energy I_3^- (center $I4d_{5/2}$)	54.8	53.83
SIBES I_3^- (terminal $I4d_{5/2}$)	1.8	
SIBES I_3^- (center $I4d_{5/2}$)	1.0	

In Table 2 the different binding energies and SIBES for I_3^- are summarized and the following can be noted: Although the absolute binding energies for I_3^- are higher than for I^-, the SIBES values derived with relation to the gas phase calculations indicate a weaker solvation for the atoms in I_3^-. Both the center and the terminal I atoms are affected by the solvation although the values are clearly stronger (almost 1 eV) for the terminal atoms. Generally the smaller SIBES observed for I_3^- compared to I^- can be accounted for in the Born framework by just assuming a cavity radius somewhere between the length and width of the I_3^- anion. However, it is equally clear that the large difference between the SIBES values for the terminal and center requires a microscopic understanding and that the specific interaction with the solvent such as hydrogen bonding will be important. Before discussing this further we will also consider the results from mixed solutions containing I^- and I_3^-.

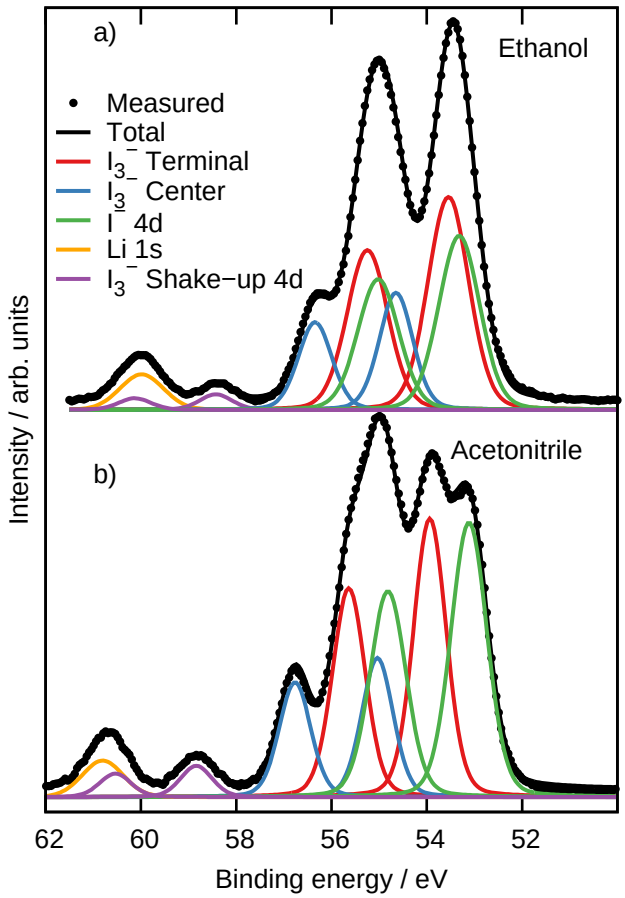

Figure 6: Experimental PES spectra of solutions with mixed I^- and I_3^- electrolytes. At the top is the ethanol based solution and at the bottom the same electrolyte but in acetonitrile. The spectrum from the solution in acetonitrile is adapted from our previous paper.[21] The measured spectra are compared to a fit in which Li^+, I^- and I_3^- species contribute.

3.2.3 Experimental results from mixed I^-/I_3^- electrolytes

Ethanol and acetonitrile solutions containing a 1:1 mixture of I^- and I_3^- were measured successfully and the spectra and results are shown in Figure 6 and Table 3. The spectra are clearly different indicating important differences in the SIBES values in the two different solvents. In the spectra of mixed anion solutions the I4d spectra contain overlapping contributions from I^- and I_3^-, including the signature of the shake-up. Before extracting the details of the binding energies of the I_3^- anion, a reliable scheme for the decomposition of the photoemission spectra into contributions from different species is needed. Based on the results of the pure anions presented in Table 1 and 2 the peak fitting were performed and is presented in Figure 6 and Table 3. Some significant differences in the spectra were observed in the different solvents concerning the SIBES.

3.2.4 Solvation of the polyatomic I_3^- anion

Table 3: Experimental binding energies and derived solvent-induced binding energy shifts (in eV) extracted from the spectrum of the mixed solutions presented in Figure 6.

	Ethanol	Acetonitrile	Gas (theory)
Binding energy I^- ($I4d_{5/2}$)	53.3	53.1	49.59
Binding energy I_3^- (terminal $I4d_{5/2}$)	53.6	53.9	51.87
Binding energy I_3^- (center $I4d_{5/2}$)	54.7	55.0	53.83
Difference I^- vs. I_3^- (terminal $I4d_{5/2}$)	0.3	0.8	
SIBES I^-	3.7	3.5	
SIBES I_3^- (terminal $I4d_{5/2}$)	1.7	2.0	
SIBES I_3^- (center $I4d_{5/2}$)	0.9	1.2	

Also in the mixed solutions the SIBES for terminal-I_3^- is 1.5-2 eV lower than the SIBES for I^- indicating that there are no interactions between the different anions in the mixture. The peaks originating from I^- are found at slightly lower binding energies in acetonitrile compared to ethanol in both the mixed solution as well as the solution containing only the I^- anion and is explained by the hydrogen bonding as discussed above. Interestingly, however, the SIBES for the I4d core levels of I^- and terminal-I_3^- are clearly different in the different solvents: the I_3^- peaks are located at lower binding energy in ethanol than in acetonitrile. More specifically, the relative I4d binding

energy difference between I4d core levels for I^- and terminal-I_3^- is 0.3 eV in ethanol and 0.8 eV in acetonitrile. What is the origin of the SIBES variations for the different anion species, and specifically for the variation in ethanol and acetonitrile? To disentangle this, the SIBES for the different ions need to be investigated separately. From these data we conclude that I_3^- is less strongly solvated than I^- and that this effect in the difference in solvation between the monoatomic and polyatomic ion is even more pronounced in ethanol. Based on the Born solvation model and comparing the charges of the different ions, one would expect that I_3^- would be less solvated compared to I^- since the net charge per atom is less in I_3^-. Such reasoning is in accordance with the experiments, see Table 3. At this point we yet again point out that the relative experimental binding energies have various origins and that the SIBES is derived from the theoretical gas phase reference, which have different values for the two anions. From the discussion of the SIBES for the single ions we found that hydrogen bonding gives an important contribution to the variation in SIBES for the two solutions. For I_3^- in ethanol one may therefore expect that donating hydrogen bonds with the charged terminal iodine atoms will be formed, which thus give a larger SIBES compared to I_3^- in acetonitrile. On the contrary, Table 3 shows that the SIBES for I_3^- are smaller in ethanol than in acetonitrile. This result thus indicate that for I_3^- the influence from hydrogen bonding in ethanol is not as important as it is for the simple I^-anion. Due to the less localized charge in the I_3^- anion, we expect the effect from hydrogen bonding on the SIBES to be significantly different than for I^-. The ordering of the I_3^- 4d SIBES in Table 3 in the different solvents rather reflects its macroscopic properties, as it agrees with the value of the dielectric constants associated with the respective solvent, with the smallest SIBES for ethanol (smallest ε).

The experimental value of the relative binding energy of the terminal and center contributions is fixed to be 1.1 eV in the fitting taken from the shift in pure LiI_3. As mentioned above, this value is smaller than the theoretical value for the isolated I_3^- ion, which is an indication of stronger solvation of the terminal atoms. The SIBES of the terminal peaks is hence larger than the corresponding SIBES for the central peaks, reducing the relative shift between the terminal and center contributions in the experimental spectra. If one formulates this result using the Born model and

together with the calculated charge distribution over the different atoms in I_3^- one can conclude that the SIBES should be at least twice as large for the terminal atoms compared to the central atom, see Table 3.

The solvent dependence for both I_3^- and I^- in acetonitrile and ethanol can not be easily explained neither in terms of the microscopic H-bonding interaction nor the macroscopic dielectric constants. In aqueous solution both the I^- and I_3^- ions are solvated by hydrogen-bonding,[21] strong enough to partially localize that charge and distort the geometry of the I_3^- ion. The shapes of the experimental I4d spectra in acetonitrile and ethanol strongly indicate that the charge is delocalized at the I_3^-. That explains the overall differences in SIBES for I^- and the terminal and center iodine atoms in I_3^-. The difference in charge distribution implies differences in the solvation strength and hence in the measured SIBES in Table 3: Both in ethanol and acetonitrile the highest SIBES is observed for the I^- anion and the lowest for the center iodine in I_3^-. Simulations of the SIBES within the DFT framework are in progress in order to rationalize the finer details in the solvent dependence in terms of explicit microscopic models of the spectra of the I_3^- ion in solution.

4. Conclusions

Due to hydrogen bonding in water and ethanol, these solvents stabilize dissolved anions differently from acetonitrile. We have shown that the presence of hydrogen bonding leads to larger solvation energies which was quantified by higher core-level binding energies for the I^- anions. We have also shown that the solvation energies for the polyatomic I_3^- is substantially smaller and that the core level shift between I^- and to I_3^- is clearly different in ethanol and acetonitrile. The variations in the binding energies reflect the differences in solvation, which is important in the understanding of the mechanism for the redox-mechanisms for the I^-/I_3^- electrolytes in different solvents. The study clearly shows the complexity in modeling solvation energies and thus specifically the difficulty in explaining and quantifying solvation for a redox couple with a simple measure parameter such as the dielectric constant.

Acknowledgement

The kind and helpful staff at the MAX IV laboratory in Lund is greatly acknowledged. The project has financial support from the Swedish Research Council (VR), the Carl Trygger Foundation, the Magnus Bergvall foundation, the STandUP for Energy program, and the Swedish Energy Agency. The computations were partly performed on resources provided by the Swedish National Infrastructure for Computing (SNIC) at the Swedish National Supercomputer Center (NSC) and the High Performance Computer Center North (HPC2N).

References

(1) Kuepper, F. C.; Feiters, M. C.; Olofsson, B.; Kaiho, T.; Yanagida, S.; Zimmermann, M. B.; Carpenter, L. J.; Luther, G. W., III; Lu, Z.; Jonsson, M.; Kloo, L. Commemorating Two Centuries of Iodine Research: An Interdisciplinary Overview of Current Research. *Angew. Chem. Int. Ed.* **2011**, *50*, 11598–11620.

(2) Kloo, L.; Rosdahl, J.; Svensson, P. H. On the Intra- and Intermolecular Bonding in Polyiodides. *Eur. J. Inorg. Chem.* **2002**, *2002*, 1203–1209.

(3) Svensson, P.; Kloo, L. A vibrational spectroscopic, structural and quantum chemical study of the triiodide ion. *J. Chem. Soc.-Dalton Trans.* **2000**, 2449–2455.

(4) Svensson, P.; Kloo, L. Synthesis, structure and bonding in polyiodide and metal iodide-iodine systems. *Chem. Rev.* **2003**, *103*, 1649–1684.

(5) O'Regan, B.; Grätzel, M. A low-cost, high-efficiency solar-cell based on dye-sensitized colloidal TiO_2 films. *Nature* **1991**, *353*, 737–740.

(6) Boschloo, G.; Hagfeldt, A. Characteristics of the Iodide/Triiodide Redox Mediator in Dye-Sensitized Solar Cells. *Acc. Chem. Res.* **2009**, *42*, 1819–1826.

(7) Hagfeldt, A.; Boschloo, G.; Sun, L.; Kloo, L.; Pettersson, H. Dye-Sensitized Solar Cells. *Chem. Rev.* **2010**, *110*, 6595–6663.

(8) Siegbahn, H. Electron-spectroscopy for chemical-analysis of liquids and solutions. *J. Phys. Chem.* **1985**, *89*, 897–909.

(9) Huang, Z.; Hua, W.; Verreault, D.; Allen, H. C. Salty Glycerol versus Salty Water Surface Organization: Bromide and Iodide Surface Propensities. *J. Phys. Chem. A* **2013**, *117*, 6346–6353.

(10) Cwiklik, L.; Andersson, G.; Dang, L. X.; Jungwirth, P. Segregation of inorganic ions at surfaces of polar nonaqueous liquids. *ChemPhysChem* **2007**, *8*, 1457–1463.

(11) Fulton, J. L.; Schenter, G. K.; Baer, M. D.; Mundy, C. J.; Dang, L. X.; Balasubramanian, M. Probing the Hydration Structure of Polarizable Halides: A Multiedge XAFS and Molecular Dynamics Study of the Iodide Anion. *J. Phys. Chem. B* **2010**, *114*, 12926–12937.

(12) Ottosson, N.; Cwiklik, L.; Söderström, J.; Björneholm, O.; Öhrwall, G.; Jungwirth, P. Increased Propensity of I-aq(-) for the Water Surface in Non-neutral Solutions: Implications for the Interfacial Behavior of H3Oaq+ and OHaq-. *J. Phys. Chem. Lett.* **2011**, *2*, 972–976.

(13) Ottosson, N.; Heyda, J.; Wernersson, E.; Pokapanich, W.; Svensson, S.; Winter, B.; Öhrwall, G.; Jungwirth, P.; Björneholm, O. The influence of concentration on the molecular surface structure of simple and mixed aqueous electrolytes. *Phys. Chem. Chem. Phys.* **2010**, *12*, 10693–10700.

(14) Tanida, H.; Watanabe, I. Dependence of EXAFS (extended X-ray absorption fine structure) parameters of iodide anions in various solvents upon a solvent parameter. *Bull. Chem. Soc. Japan* **2000**, *73*, 2747–2752.

(15) Kim, K. H.; Lee, J. H.; Kim, J.; Nozawa, S.; Sato, T.; Tomita, A.; Ichiyanagi, K.; Ki, H.; Kim, J.; Adachi, S.-i.; Ihee, H. Solvent-Dependent Molecular Structure of Ionic Species Directly Measured by Ultrafast X-Ray Solution Scattering. *Phys. Rev. Lett.* **2013**, *110*, 165505–165509.

(16) Arbman, M.; Holmberg, S.; Lundholm, M.; Siegbahn, H.; Gropen, O.; Wahlgren, U. Liquid ESCA Measurements and ECP Calculations on the 3D Spectrum of I_3^-. *Chem. Phys.* **1983**, *81*, 113–119.

(17) Markovich, G.; Giniger, R.; Levin, M.; Cheshnovsky, O. Photoelectron-Spectroscopy of Iodine Anion Solvated in Water Clusters. *J. Chem. Phys.* **1991**, *95*, 9416–9419.

(18) Margulis, C.; Coker, D.; Lynden-Bell, R. Symmetry breaking of the triiodide ion in acetonitrile solution. *Chem. Phys. Lett.* **2001**, *341*, 557–560.

(19) Margulis, C.; Coker, D.; Lynden-Bell, R. A Monte Carlo study of symmetry breaking of I_3^- in aqueous solution using a multistate diabatic Hamiltonian. *J. Chem. Phys.* **2001**, *114*, 367–376.

(20) Marcus, Y. The properties of organic liquids that are relevant to their use as solvating solvents. *Chem. Soc. Rev.* **1993**, *22*, 409–416.

(21) Josefsson, I.; Eriksson, S. K.; Ottosson, N.; Öhrwall, G.; Siegbahn, H.; Hagfeldt, A.; Rensmo, H.; Björneholm, O.; Odelius, M. Collective Hydrogen Bond Dynamics Dicates the Electronic Structure of Aqueous I_3^-. *Phys. Chem. Chem. Phys.* **2013**, *15*, 20189–20196.

(22) Johnson, A. E.; Myers, A. B. Solvent Effects in the Raman Spectra of the Triiodide Ion: Observation of Dynamic Symmetry Breaking and Solvent Degrees of Freedom. *J. Phys. Chem.* **1996**, *100*, 7778–7788.

(23) Hufner, S. *Photoelectron Spectroscopy- Principles and Applications*; Springer, 2003.

(24) Bergersen, H.; Marinho, R. R. T.; Pokapanich, W.; Lindblad, A.; Björneholm, O.; Sæthre, L. J.; Öhrwall, G. A photoelectron spectroscopic study of aqueous tetrabutylammonium iodide. *J. Phys.-Cond. Matt.* **2007**, *19*, 326101–326109.

(25) Kimura, K. *Handbook of HeI photoelectron spectra of fundamental organic molecules*; Japan Scientific Societies Press, 1981.

(26) Faubel, M.; Steiner, B.; Toennies, J. Photoelectron spectroscopy of liquid water, some alcohols, and pure nonane in free micro jets. *J. Chem. Phys.* **1997**, *106*, 9013–9031.

(27) Berrah, N.; Bliodeau, R.; Ackerman, G.; Bozek, J.; Turri, G.; Kukk, E.; Cheng, W.; Snell, G. Probing atomic and molecular dynamics from within. *Rad. Phys. Chem.* **2004**, *70*, 491–500, Indo/United States Workshop on Radiation Physics with Synchrotrons and Other New Sources, Argonne Natl Lab, Argonne, IL, May 13-16, 2003.

(28) Ausmees, A.; Osborne, S. J.; Moberg, R.; Svensson, S.; Aksela, S.; Sairanen, O.-P.; Kivimäki, A.; Naves de Brito, A.; Nõmmiste, E.; Jauhiainen, J.; Aksela, H. High-resolution study of the Xe $4d_{5/2}$:$4d_{3/2}$ branching ratio. *Phys. Rev. A* **1995**, *51*, 855–858.

(29) Aquilante, F.; De Vico, L.; Ferré, N.; Ghigo, G.; Malmqvist, P.-Å.; Neogrády, P.; Pedersen, T. B.; Pitonak, M.; Reiher, M.; Roos, B. O.; Serrano-Andrés, L.; Urban, M.; Veryazov, V.; Lindh, R. MOLCAS 7: The Next Generation. *J. Comp. Chem.* **2010**, *31*, 224–247.

(30) Finley, J.; Malmqvist, P.-Å.; Roos, B. O.; Serrano-Andrés, L. The Multi-State CASPT2 Method. *Chem. Phys. Lett.* **1998**, *288*, 299–306.

(31) Roos, B. O.; Taylor, P. R.; Siegbahn, P. E. M. A Complete Active Space SCF Method (CASSCF) Using a Density-matrix Formulated Super-CI Approach. *Chem. Phys.* **1980**, *48*, 157–173.

(32) Roos, B. O. In *Advances in Chemical Physics; Ab Initio Methods in Quantum Chemistry - II*; Lawley, K. P., Ed.; John Wiley & Sons Ltd.: Chichester, England, 1987; Chapter 69, p 399.

(33) Roos, B. O.; Lindh, R.; Malmqvist, P.-Å.; Veryazov, V.; Widmark, P.-O. Main Group Atoms and Dimers Studied with a New Relativistic ANO Basis Set. *J. Phys. Chem. A* **2004**, *108*, 2851–2858.

(34) Roos, B. O.; Lindh, R.; Malmqvist, P.-Å.; Veryazov, V.; P.-O-Widmark, New relativistic ANO basis sets for actinide atoms. *Chem. Phys. Lett.* **2005**, *409*, 295–299.

(35) Roos, B. O.; Lindh, R.; Malmqvist, P.-Å.; Veryazov, V.; Widmark, P.-O.; Borin, A. C. New relativistic ANO basis sets for lanthanide atoms with applications to the Ce diatom and LuF_3. *J. Phys. Chem. A* **2008**, *112*, 11431–11435.

(36) Roos, B. O.; Veryazov, V.; Widmark, P.-O. Relativistic ANO type basis sets for the alkaline and alkaline earth atoms applied to the ground state potentials for the corresponding dimers. *Theor. Chim. Acta* **2004**, *111*, 345–351.

(37) Andersson, K.; Malmqvist, P.-Å.; Roos, B. O. Second-Order Perturbation Theory with a Complete Active Space Self-Consistent Field Reference Function. *J. Chem. Phys.* **1992**, *96*, 1218–1226.

(38) Gagliardi, L.; Lindh, R.; Karlström, G. Local properties of quantum chemical systems: the LoProp approach. *J. Chem. Phys.* **2004**, *121*, 4494–4500.

(39) Douglas, N.; Kroll, N. M. Quantum Electrodynamical Corrections to Fine-structure of Helium. *Ann. Phys.* **1974**, *82*, 89–155.

(40) Hess, B. Relativistic Electronic-structure Calculations Employing a 2-component No-pair Formalism with External-field Projection Operators. *Phys. Rev. A* **1986**, *33*, 3742–3748.

(41) Malmqvist, P.-Å. Calculation of Transition Density Matrices by Non-Unitary Orbital Transformations. *Int. J. Quantum Chem.* **1986**, *30*, 479–494.

(42) Malmqvist, P.-Å.; Roos, B. O. The CASSCF State Interaction Method. *Chem. Phys. Lett.* **1989**, *155*, 189–194.

(43) Tomasi, J.; Mennucci, B.; Cammi, R. Quantum mechanical continuum solvation models. *Chem. Rev.* **2005**, *105*, 2999–3093.

(44) Barone, V.; Cossi, M.; Tomasi, J. A new definition of cavities for the computation of solvation free energies by the polarizable continuum model. *J. Chem. Phys.* **1997**, *107*, 3210–3221.

(45) Toukan, K.; Rahman, A. Molecular-Dynamics Study of Atomic Motions in Water. *Phys. Rev. B* **1985**, *31*, 2643–2648.

(46) Jorgensen, W.; Maxwell, D.; TiradoRives, J. Development and testing of the OPLS all-atom force field on conformational energetics and properties of organic liquids. *J. Am. Chem. Soc.* **1996**, *118*, 11225–11236.

(47) Nikitin, A.; Lyubartsev, A. New six-site acetonitrile model for simulations of liquid acetonitrile and its aqueous mixtures. *J. Comput. Chem.* **2007**, *28*, 2020–2026.

(48) Heinzinger, K. Computer simulations of aqueous electrolyte solutions. *Physica B+C* **1985**, *131*, 196–216.

(49) Kjeldsen, H.; Andersen, P.; Folkmann, F.; Hansen, J.; Kitajima, M.; Andersen, T. Experimental study of 4f wavefunction contraction: 4d-photoionization of low-charged ions of I, Xe, Cs and Ba. *J. Phys. B* **2002**, *35*, 2845–2860.

(50) Siegbahn, H.; Lundholm, M.; Arbman, M.; Holmberg, S. Core electron-spectroscopy of negative-ions in solution. *Physica Scripta* **1984**, *30*, 305–308.

(51) Mathews, R.; Key, R.; Sur, A.; Ewig, C.; Banna, M. On the core binding-energies of ions - the 3d levels of I^- and CS^+. *J. Chem. Phys.* **1981**, *74*, 5407–5410.

(52) Born, M. Volumes and heats of hydration of ions. *Z. Phys.* **1920**, *1*, 45–48.

(53) Weber, R.; Winter, B.; Schmidt, P.; Widdra, W.; Hertel, I.; Dittmar, M.; Faubel, M. Photoemission from aqueous alkali-metal-iodide salt solutions using EUV synchrotron radiation. *J. Phys. Chem. B* **2004**, *108*, 4729–4736.

(54) Ottosson, N.; Børve, K. J.; Spångberg, D.; Bergersen, H.; Sæthre, L. J.; Faubel, M.; Pokapanich, W.; Öhrwall, G.; Björneholm, E.; Winter, B. On the Origins of Core-Electron Chemical Shifts of Small Biomolecules in Aqueous Solution: Insights from Photoemission and ab Initio Calculations of Glycine(aq). *J. Am. Chem. Soc.* **2011**, *133*, 3120–3130.

(55) Rashin, A.; Honig, B. Reevaluation of the Born model of ion hydration. *J. Phys. Chem.* **1985**, *89*, 5588–5593.

(56) Winter, B.; Weber, R.; Hertel, I.; Faubel, M.; Jungwirth, P.; Brown, E.; Bradforth, S. Electron binding energies of aqueous alkali and halide ions: EUV photoelectron spectroscopy of liquid solutions and combined ab initio and molecular dynamics calculations. *J. Am. Chem. Soc.* **2005**, *127*, 7203–7214.

(57) Ågren, H.; Mikkelsen, K. V. Theory of solvent effects on electronic spectra. *J. Mol. Struct. Theochem* **1991**, *234*, 425–467.